

Order-by-disorder in the XY pyrochlore antiferromagnet revisited

Pawel Stasiak,^{1,2} Paul A. McClarty,^{1,3} and Michel J. P. Gingras^{1,4}

¹*Department of Physics and Astronomy, University of Waterloo, Waterloo, ON, N2L 3G1, Canada.*

²*Department of Mathematics, University of Reading, Whiteknights, PO Box 220, Reading RG6 6AX, UK.*

³*Max Planck Institute for the Physics of Complex Systems, Nöthnitzer Str. 13, Dresden, 01187, Germany.*

⁴*Canadian Institute for Advanced Research, 180 Dundas Street West, Suite 1400, Toronto, ON, M5G 1Z8, Canada.*

(Dated: September 1, 2011)

We investigate the properties of the XY pyrochlore antiferromagnet with local $\langle 111 \rangle$ planar anisotropy. We find the ground states and show that the configurational ground state entropy is subextensive. By computing the free energy due to harmonic fluctuations and by carrying out Monte Carlo simulations, we confirm earlier work indicating that the model exhibits thermal order-by-disorder leading to low temperature long-range order consisting of discrete magnetic domains. We compute the spin wave spectrum and show that thermal and quantum fluctuations select the same magnetic structure. Using Monte Carlo simulations, we find that the state selected by thermal fluctuations in this XY pyrochlore antiferromagnet can survive the addition of sufficiently weak nearest-neighbor pseudo-dipolar interactions to the spin Hamiltonian. We discuss our results in relation to the $\text{Er}_2\text{Ti}_2\text{O}_7$ pyrochlore antiferromagnet.

PACS numbers: 75.10.Dg 75.10.Jm 75.40.Cx 75.40.Gb

I. INTRODUCTION

The geometric frustration of magnetic interactions on lattices of magnetic moments often leads to a configurational classical ground state entropy that scales with the volume of the system, V , as V^α with $0 < \alpha \leq 1$. This can have some unusual consequences. A well known example is the Ising model on the triangular lattice with nearest-neighbor antiferromagnetic interactions which has an extensive ground state entropy and exhibits no finite temperature transition.¹ While in real materials a V^α entropy left by the leading interactions is often energetically lifted by weaker interactions, leading to long-range magnetic order, there are some exceptions. For example, in the $\text{Dy}_2\text{Ti}_2\text{O}_7$ and $\text{Ho}_2\text{Ti}_2\text{O}_7$ spin ice materials,² in which the magnetic moments are described by Ising spins, the extensive ($\alpha = 1$) low temperature entropy caused by frustration of the leading effective ferromagnetic nearest-neighbor interactions is indeed lifted by the perturbing long-ranged part of the dipolar interaction.^{3–5} However, the degeneracy lifting in this system is so weak that the theoretically expected phase transition to magnetic long-range order is inhibited by a freezing into a spin ice state without long-range order.^{6,7}

Another possibility in a system with an exponentially ($\exp[CV^\alpha]$) large number of classical degenerate ground states is that thermal or quantum fluctuations might select a subset of states about which the density of zero modes is greatest. These entropic and quantum state selection mechanisms are both referred to as order-by-disorder.^{8–11} Among pyrochlore antiferromagnets, in which the spins sit on a lattice of corner-sharing tetrahedra, Moessner and Chalker have given a criterion for the occurrence of long-range order induced by thermal fluctuations.¹² This criterion is based on the degree of divergence of the statistical weight of particular spin configurations – a power-counting argument depending on the number of zero energy excitations (zero modes) for a given spin configuration and the number of dimensions of the ground state manifold. For example, this criterion indicates that the XY antiferromagnet with globally coplanar

spins (spins perpendicular to the global $[001]$ axis) should exhibit entropic selection – a result which is borne out by Monte Carlo simulations.¹² For such XY systems, this comes about because the number of zero modes about collinear spin configurations is proportional to the number of spins whereas the configurational entropy in the ground state is subextensive, growing as $V^{2/3}$.^{12,13}

This article is concerned with the pyrochlore XY antiferromagnet with local $\langle 111 \rangle$ spins meaning that there is a different easy plane for each of the four tetrahedral sublattices.^{13–16} Because such a model preserves the cubic symmetry of the pyrochlore lattice and because the single ion crystal field can, and does in various materials,¹⁷ generate such an anisotropy, it is more physical than the aforementioned pyrochlore XY model with a global easy axis.¹² The model has been recognized to exhibit a continuous degeneracy in its classical ground state.^{15,16} Monte Carlo simulations of the local $\langle 111 \rangle$ XY antiferromagnet^{13,15,16} indicate that it exhibits two phases – a high temperature paramagnetic phase and a low temperature long-range ordered phase. We refer to the magnetic structure in the ordered phase as ψ_2 to be consistent with Ref. [18] and the group theory literature. A calculation of the spectrum of the Hessian about different discrete ground states¹⁵ suggests that the observed long-range ordered spin configuration in Monte Carlo simulations has the largest density of zero modes of all the degenerate ground states and, consequently, that the observed transition is an example of classical (thermal) OBD.^{15,16} However, it has been suggested that selection of the long-range ordered ψ_2 state might not survive in the thermodynamic limit.¹⁵

In this article, we give a systematic account of the properties of the local $\langle 111 \rangle$ XY pyrochlore. We present in Section II the model and its ground states. In Section III, we discuss some of the details of the Monte Carlo simulations performed in this work. Section IV reports results of an analytical and numerical investigation of the thermal order-by-disorder mechanism, providing strong evidence that the fluctuation selection mechanism of the ψ_2 state does survive in the ther-

modynamic limit and giving further insight into its physical origin. We also include in Section IV a subsection showing that there is a quantum order-by-disorder mechanism in the XY model as speculated but not shown in Ref. [14]. Finally, in Section V, we describe the material $\text{Er}_2\text{Ti}_2\text{O}_7$ which is an easy plane antiferromagnet exhibiting the ψ_2 structure in its ordered phase^{14,18} and which provides an experimental motivation for studying this model. In particular, we discuss the effect of weak dipolar interaction on the XY antiferromagnet and the problem this interaction poses for understanding the long-range ordered phase of $\text{Er}_2\text{Ti}_2\text{O}_7$ with ψ_2 structure.^{14,18}

II. MODEL

In this work, we mostly focus on the problem of the zero and finite temperature behavior of interacting classical spins of length $|\mathbf{S}| = 1$ on the sites of a pyrochlore lattice of corner-sharing tetrahedra with an infinite single-ion anisotropy such that the spins lie within their respective local XY planes perpendicular to the local $\langle 111 \rangle$ directions. In Section IV B, we discuss the problem of order-by-disorder due to quantum fluctuations in a model with spin operators \mathbf{S} .^{13–15}

The interactions are taken to be antiferromagnetic isotropic exchange between nearest neighbors with coupling J ($J > 0$). Later on we also consider, as a perturbation, pseudo-dipolar interactions solely between nearest neighbours and with coupling strength \mathcal{D} . Thus the Hamiltonian is taken to be

$$H = J \sum_{\langle i,j \rangle} \mathbf{S}_i \cdot \mathbf{S}_j + \mathcal{D} R_{\text{nn}}^3 \sum_{\langle i,j \rangle} \frac{\mathbf{S}_i \cdot \mathbf{S}_j}{|\mathbf{R}_{ij}|^3} - \frac{3(\mathbf{S}_i \cdot \mathbf{R}_{ij})(\mathbf{S}_j \cdot \mathbf{R}_{ij})}{|\mathbf{R}_{ij}|^5} \quad (1)$$

where R_{nn}^3 is the nearest-neighbor distance.

Consider first the exchange-only model with $\mathcal{D} = 0$. In this case, the Hamiltonian in Eq. (1) can be put into the form $H_{\text{ex}} = J \sum_{\text{t}} (\mathbf{S}_{\text{t}}^2 - 4S^2)$, where the sum runs over all connected tetrahedra¹² and \mathbf{S}_{t} is the total spin on each tetrahedron. It follows that the ground states are all those states with zero net magnetic moment ($\mathbf{S}_{\text{t}} = 0$) on each tetrahedron. Therefore, we write down the conditions for the three components of the total moment on a tetrahedron to be zero. In doing so, we impose the XY constraint so that the orientation of spin a , (for sublattices $a = 1, 2, 3, 4$), is given by a single angle ϕ_a measured with respect to axes within the local plane (normal to the relevant local $[111]$ direction) given in Ref. [19]. The condition of zero moment on each tetrahedron can then be written as

$$\begin{aligned} \cos(\phi_1) + \cos(\phi_2) &= \cos(\phi_3) + \cos(\phi_4) \\ \cos(\phi'_1) + \cos(\phi'_3) &= \cos(\phi'_2) + \cos(\phi'_4) \\ \cos(\phi''_1) + \cos(\phi''_4) &= \cos(\phi''_2) + \cos(\phi''_3), \end{aligned}$$

where $\phi'_a \equiv \phi_a + \frac{2\pi}{3}$ and $\phi''_a \equiv \phi_a + \frac{4\pi}{3}$. There are four solution branches to these equations. Each branch corresponds to a continuous degeneracy wherein all four spins are rotated smoothly within their respective local $[111]$ XY plane.

We place an overbar on ϕ_a ($\bar{\phi}_a$) to signify the angle for sublattice a giving an energy minimum (zero moment on each

tetrahedron). Then, we label these branches in the following way:

$$\begin{aligned} \text{Branch 1 : } \bar{\phi} &\equiv \bar{\phi}_1 = \bar{\phi}_2 = \bar{\phi}_3 = \bar{\phi}_4 \\ \text{Branch 2 : } \bar{\phi} &\equiv \bar{\phi}_1 = \bar{\phi}_2 = -\bar{\phi}_3 = -\bar{\phi}_4 \\ \text{Branch 3 : } \bar{\phi} &\equiv \bar{\phi}_1 = \bar{\phi}_3, \quad \frac{2\pi}{3} - \bar{\phi} = \bar{\phi}_2 = \bar{\phi}_4 \\ \text{Branch 4 : } \bar{\phi} &\equiv \bar{\phi}_1 = \bar{\phi}_4, \quad \frac{4\pi}{3} - \bar{\phi} = \bar{\phi}_2 = \bar{\phi}_3. \end{aligned} \quad (2)$$

A further discussion of these solutions can be found in Appendix A.

To enumerate all the ground states on the pyrochlore lattice we first tile all the tetrahedra with a particular spin configuration from Branch 1. Then, we choose a line of nearest-neighbor spins traversing the length L of the system. The sublattice labels of the spins on the chain alternate between two values a and b . There are six such pairs of labels. One can then transform the spins along the chain so that the spin configurations of the associated tetrahedra belong to another branch of solutions. For example, consider a single chain made of sublattices 3 and 4. All the local angles along this chain are identical initially and equal to, say θ . We can transform these to $-\theta$ with no energy cost. Therefore, the entropy within the ground state manifold scales as L^2 as first noted in Ref. [13]. This is in contrast to both the Heisenberg pyrochlore antiferromagnet and the global easy axis (Ising) pyrochlore antiferromagnet both of which have an extensive entropy.

We note that the four branches in Eq. (2) intersect in pairs. These intersection points are at special sublattice angles $\bar{\phi} = n\pi/3$ with integer n . We refer to these as ψ_2 states in the rest of this article. By exploiting these intersection angles to move between the branches, one can smoothly visit all the ground states on a single tetrahedron and, indeed, on the whole pyrochlore lattice. If we return to the above chain of sublattices #3 and #4, the $\bar{\phi} = 0$ configuration allows the tetrahedra along this chain to pass smoothly from Branch 1 to Branch 2. As shown in Refs. [14,15] and in Section IV below, thermal fluctuations have the effect of selecting a magnetic structure with $\mathbf{q} = 0$ ordering wavevector and spin orientations at these discrete $\bar{\phi}$ angles. There are six distinct ψ_2 ground states which are the six $\mathbf{q} = 0$ ordered states with tetrahedra tiled with local angles $\bar{\phi}_a = n\pi/3$ for sublattices $a = 1, 2, 3, 4$ and with integer n . One can take the observation that the lattice zero modes are along sublattice chains to understand an aspect of the Monte Carlo results of Ref. [15]; in particular, the finite-size scaling of the average energy of the ψ_2 states at low temperature. Since this point is somewhat removed from the main story of the paper, we present the argument in Appendix C.

When $\mathcal{D} \neq 0$, the continuous ground state degeneracy of the exchange only model is “immediately” replaced with a discrete global degeneracy with $\mathbf{q} = 0$ ordering wavevector selected from the manifold of states described above. These energetically selected states are referred to as the ψ_4 states¹⁸ or Palmer-Chalker states in the literature after Ref. [20]. The

angles specifying the ψ_4 states are

$$\begin{aligned} \text{State 1 : } \bar{\phi}_1 = \bar{\phi}_2 = \frac{\pi}{2} & \quad \bar{\phi}_3 = \bar{\phi}_4 = \frac{3\pi}{2} \\ \text{State 2 : } \bar{\phi}_1 = \bar{\phi}_4 = \frac{7\pi}{6} & \quad \bar{\phi}_2 = \bar{\phi}_3 = \frac{\pi}{6} \\ \text{State 3 : } \bar{\phi}_1 = \bar{\phi}_3 = \frac{11\pi}{6} & \quad \bar{\phi}_2 = \bar{\phi}_4 = \frac{5\pi}{6} \end{aligned} \quad (3)$$

and the time-reversed configurations. In anticipation of what follows in Section V, we note that the ψ_4 states are the ground states one finds for antiferromagnetic nearest-neighbor exchange with sufficiently weak nearest-neighbor pseudo-dipolar as well as for true $1/r^3$ long-range magnetostatic dipolar interactions in the classical Heisenberg pyrochlore antiferromagnet model.^{20–22} Interestingly, the ψ_4 states are found experimentally to be the ground state of the $\text{Gd}_2\text{Sn}_2\text{O}_7$ pyrochlore antiferromagnet,²³ but not of the closely related $\text{Gd}_2\text{Ti}_2\text{O}_7$ material.²⁴

III. MONTE CARLO METHOD

In Sections IV C and V below, we report results from Monte Carlo simulations of the local $\langle 111 \rangle$ XY pyrochlore antiferromagnet. In this section, we give details of the Monte Carlo algorithm and the observables that were measured in the Monte Carlo simulations.

The Monte Carlo simulations were performed using parallel tempering²⁵ in which N_T replicas of a system of N spins, each at a different temperature and with a different series of pseudo-random numbers, are simulated simultaneously. In addition to local spin moves, parallel tempering swaps that exchange configurations between a pair of temperatures are attempted. The configuration swap attempts are accepted or rejected based on a Metropolis condition that preserves detailed balance. Parallel tempering has been shown, in systems known to equilibrate slowly using other methods, to improve performance substantially.²⁵ Replica swaps are attempted with a frequency of one attempt every 100 local Monte Carlo sweeps. A local Monte Carlo sweep consists of N spin move attempts. In our simulations, $N_T = 64$ with either a constant increment between the temperatures, or with the temperatures self consistently adjusted to obtain a uniform parallel tempering acceptance rate.

With each spin carrying a single angular coordinate ϕ_i , the local spin moves involve choosing an angle increment $\delta\phi_i$ from a uniform distribution between $-\delta\phi_{\max}$ and $\delta\phi_{\max}$. The angle of spin \mathbf{S}_i was updated to $\phi_i + \delta\phi_i$ and each tentative spin rotation was accepted or rejected based on a Metropolis test. The maximum increment $\delta\phi_{\max}$ was updated every 100 Monte Carlo moves in order to maintain the spin move acceptance rate at 50%.

Physical observables were computed every 100 Monte Carlo sweeps. To determine the presence of long-range order with ordering wavevector $\mathbf{q} = 0$ (expected for sufficiently small \mathcal{D}/J in the model discussed above^{20–22}), the sublattice magnetization was computed¹³

$$M_4 = \left\langle \sqrt{\frac{1}{4} \sum_{a=1}^4 \left(\frac{1}{N_P} \sum_{i=1}^{N_P} \mathbf{S}_{i,a} \right)^2} \right\rangle_{\text{th}}, \quad (4)$$

where each spin carries an fcc lattice label i and a sublattice label a (see Ref. [26]) and the number of sites in the lattice is $N \equiv 4N_P$, where N_P is the number of fcc sites. The angled brackets $\langle \dots \rangle_{\text{th}}$ denote a thermal average. In order to distinguish the ψ_2 (Refs. [14,18]) and ψ_4 (Refs. [18,20]) phases, we introduce unit vectors $\hat{\mathbf{e}}_a^{(\gamma(d))}$ which are oriented in the expected spin directions on each sublattice a for magnetic structure identified by the label γ with the domains labelled d , for both the $\gamma = \psi_2$ and $\gamma = \psi_4$ structures. From the combination

$$\Psi^{(\gamma(d))} = \frac{1}{N_P} \sum_{i=1}^{N_P} \sum_{a=1}^4 \mathbf{S}_{i,a} \cdot \hat{\mathbf{e}}_a^{(\gamma(d))}, \quad (5)$$

we compute the order parameter

$$q_\gamma = \left\langle \sum_d \left(\Psi^{(\gamma(d))} \right)^2 \right\rangle_{\text{th}}, \quad (6)$$

for the $\gamma = \psi_2$ (Refs. [14,18]) and $\gamma = \psi_4$ (Refs. [18,20]) magnetic structures. In Eq. (6), the sum is taken over a choice of three out of the six magnetic domains, for each of these two structures, which are not related to one another by time reversal. The spin directions corresponding to the domains for ψ_4 and ψ_2 are given in Section II. — for ψ_4 in Eq. (3) and for ψ_2 we have all angles $\bar{\phi}_a = n\pi/3$. The order parameter for ψ_4 , q_{ψ_4} , is the same one computed in the simulations of Ref. [27]. The magnetic specific heat per spin was computed from the fluctuations in the total energy of the system.

The sensitivity of the results to the initial spin configurations was assessed by comparing the results of simulations starting from (i) random configurations with a different configuration for each thermal replica, (ii) ψ_2 ordered states and (iii) ψ_4 ordered states. To ensure that equilibration was reached for each simulation, we checked that the results were independent of initial conditions. Also, the evolution of the order parameters was monitored during the course of each simulation to ensure that they reached a stationary state before the statistics were collected. Equilibration issues are discussed further in Sections IV C and V.

IV. ORDER-BY-DISORDER

In this section, we consider the exchange-only model ($\mathcal{D} = 0$) given in Eq. (1). General arguments given in Ref. [12] indicate that the XY antiferromagnet with coplanar spins should exhibit a thermally driven order-by-disorder transition. This argument does not straightforwardly carry over to the non-coplanar $\langle 111 \rangle$ XY antiferromagnet. Simulation evidence for thermal order-by-disorder in the local $\langle 111 \rangle$ XY model transition was presented in Refs. [13–16]. The classical degeneracies of this model were identified in Ref. [15] and order-by-disorder was found via Monte Carlo simulations. However,

the possibility was mentioned in Ref. [15] that the temperature at which long-range order with a nonzero ψ_2 order parameter develops might vanish in the thermodynamic limit. We present simulation results which provide compelling evidence that, for the exchange-only ($\mathcal{D} = 0$) model, a first order phase transition to a long-range ordered ψ_2 state persists in the thermodynamic limit. We begin, however, with a previously unreported calculation of the free energy including only harmonic fluctuations which exposes a thermal ψ_2 order-by-disorder in the thermodynamic limit. Then, having investigated the order-by-disorder mechanism in the exchange-only ($\mathcal{D} = 0$) model, we discuss in Section V the effect of competing nearest-neighbor pseudo-dipolar ($\mathcal{D} \neq 0$) interactions in this model.

A. Computation of the free energy

In this section, we show that certain discrete spin configurations from the manifold of $\mathbf{q} = 0$ ground states minimize the free energy computed from harmonic fluctuations about the classical ground states. We assume that every tetrahedron on the lattice is tiled with the same spin configuration (*i.e.* that the ordering wavevector is $\mathbf{q} = 0$). If we constrain the ordering to be $\mathbf{q} = 0$, the spin configuration is fixed by specifying four angles ϕ_a - one for each sublattice. Let the angles in a ground state configuration be denoted $\bar{\phi}_a$ for which the ground state energy is $H(\bar{\phi}_a) = NE_g$, where N is the number of spins. We then we consider small fluctuations $\delta\phi_i$ about these angles $\phi_i = \bar{\phi}_i + \delta\phi_i$. The terms linear in $\delta\phi_i$ vanish, so the Hamiltonian $H = NE_g + H_2 + \dots$, where H_2 is the part harmonic in the angular deformations. H_2 is written in \mathbf{k} space as $H_2 = \sum_{\mathbf{k}, a, b} \delta\phi_a(\mathbf{k}) A^{ab}(\mathbf{k}) \delta\phi_b(-\mathbf{k})$. Here, $\delta\phi_a(\mathbf{k}) = (1/\sqrt{N_P}) \sum_{\mathbf{R}_\mu} \exp(i\mathbf{k} \cdot (\mathbf{R}_\mu + \mathbf{r}_a)) \delta\phi_a(\mathbf{R}_\mu)$, where \mathbf{R}_μ are the fcc lattice points and \mathbf{r}_a are the vectors for the tetrahedral basis (see Ref. [26] for notation convention). This choice of convention for the lattice labelling ensures that the Hessian $A^{ab}(\mathbf{k})$ is real. The eigenvalues $\lambda_A(\mathbf{k})$ of $A^{ab}(\mathbf{k})$ are nonnegative, reflecting the stability of the ground states. The spectrum of A^{ab} is computed in \mathbf{k} space as a function of the ground state for each branch.

One finds that for the special minimum energy configurations $\bar{\phi}_a = n\pi/3$ for $a = 1, 2, 3, 4$, the four eigenvalues, $\lambda_A(\mathbf{k})$, ($A = 1, 2, 3, 4$) of the $A^{ab}(\mathbf{k})$ Hessian take the form

$$\begin{array}{ll} \bar{\phi}_a = 0, \pi & \lambda_A = 1 \pm \cos(\mathbf{k} \cdot \mathbf{r}_{12}), 1 \pm \cos(\mathbf{k} \cdot \mathbf{r}_{34}) \\ \bar{\phi}_a = \pi/3, 4\pi/3 & \lambda_A = 1 \pm \cos(\mathbf{k} \cdot \mathbf{r}_{13}), 1 \pm \cos(\mathbf{k} \cdot \mathbf{r}_{24}) \\ \bar{\phi}_a = 2\pi/3, 5\pi/3 & \lambda_A = 1 \pm \cos(\mathbf{k} \cdot \mathbf{r}_{23}), 1 \pm \cos(\mathbf{k} \cdot \mathbf{r}_{14}) \end{array}$$

where each row gives the four eigenvalues for the indicated particular set of $\bar{\phi}_a$ ($a = 1, 2, 3, 4$) angles and which correspond to the aforementioned ψ_2 states. The vector \mathbf{r}_{ab} joins nearest neighbors with sublattice labels a and b . The ψ_2 states are distinguished from the other ground states in having a much higher density of zero modes - 2 planes of zero modes in the first Brillouin zone.^{15,16} The planes come about because, at these angles, one can smoothly introduce defects into the system along (what are usually referred to as α and β) chains

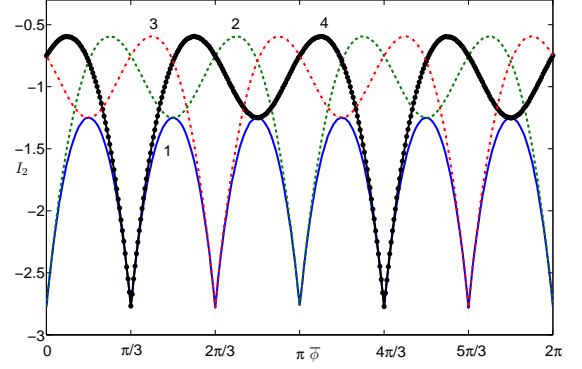


FIG. 1: (Color online) Plot showing the harmonic free energy contribution I_2 for each of the four branches ($A = 1, 2, 3, 4$) of ground states with the $\bar{\phi}_a$ angle for each sublattice $a = 2, 3, 4$ expressed in terms of $\bar{\phi}_1$ via the parametrization given in Eq. (2). Each of the four curves is labelled by its ground state branch number taken from Eq. (2). Note therefore that the horizontal axis does not identify a unique spin configuration but rather a unique configuration for each of the four branches. The minima in the free energy appear where pairs of ground state branches meet - at the ψ_2 spin configurations.

in the crystal as described in Section II. At angles away from the ψ_2 states, one can still introduce chain defects but not continuously.

We now compute the free energy for each $\mathbf{q} = 0$ configuration after dropping all terms in the Hamiltonian beyond the harmonic terms. The free energy $F[\bar{\phi}]$ at inverse temperature, β , is given at the harmonic level by

$$F[\bar{\phi}] \approx NE_g - \frac{1}{\beta} \log \left[\left(\prod_{a, \mathbf{k}} \int d[\delta\phi_a(\mathbf{k})] \right) \exp(-\beta H_2) \right] \quad (7)$$

and hence

$$F[\bar{\phi}] \approx NE_g - \frac{N}{2\beta} \log \left(\frac{\pi}{\beta} \right) + \frac{1}{2\beta} \sum_{\mathbf{k}} \log(\det A(\mathbf{k})). \quad (8)$$

In the limit as $N \rightarrow \infty$, the third (last) term on the right hand side of Eq. (8) is $\frac{N}{4} \frac{1}{(2\pi)^3} I_2$ with $I_2 = \sum_A \int d^3\mathbf{k} \log(\lambda_A(\mathbf{k}))$ for the four ground state branches given in Section II (see Appendix B for a discussion of the various prefactors of I_2). We evaluate the integral numerically using a Monte Carlo method with 10^8 points, noting that the singularities for the ψ_2 spin configurations are integrable because the integrals take the form $\int_0^c dk \log k$ for some constant c .²⁸ The results are shown in Fig. 1. Evidently, I_2 , and consequently the free energy $F[\bar{\phi}]$, is minimized for the ψ_2 states at $\bar{\phi}_a = n\pi/3$ where pairs of branches meet.

It is often the case that one can simulate the effect of order-by-disorder by introducing a term into the Hamiltonian of the form

$$H_{\text{OBD}} = -|\Gamma| \sum_{i,j} (\mathbf{S}_i \cdot \mathbf{S}_j)^2, \quad (9)$$

that selects the most collinear spin configurations among the classical ground states (see, for example, Refs. [8–10]). The usual argument for the selection of such states is that collinear spin configurations have, among all states, fluctuations that couple most strongly because fluctuations are responsible for effective fields perpendicular to the spin direction even in the broken symmetry phase. The local XY and zero moment constraints of the XY pyrochlore antiferromagnet ensure that the spins cannot be collinear, but it is interesting to ask whether the ψ_2 configurations are the most collinear states within the set of ground states. One finds that Eq. (9) is constant within the whole ground state manifold of Eq. (2). However, the sum $-\sum_{i,j} |\mathbf{S}_i \cdot \mathbf{S}_j|$ is minimized by the ψ_2 states which lends some credence to the intuition that the most collinear states among all the classically degenerate zero temperature ground states must be selected.

B. Quantum selection

Having shown that thermal fluctuations select the ψ_2 states, we now turn to the effect of quantum fluctuations which, in general, need not select the same states. In this section, we present the spin wave spectrum computed using the Holstein-Primakoff transformation treated in a large S expansion and truncated at harmonic order. The calculation is performed for the Hamiltonian in Eq. (1) with $D = 0$. In the coordinate system with z axes taken along the $\langle 111 \rangle$ directions, the Hamiltonian is written $H = \sum \mathcal{J}_{ij}^{\alpha\beta} S_i^\alpha S_j^\beta$ where α and β denote the spin components. The local Ising components of the matrix of interactions $\mathcal{J}_{ij}^{\alpha\beta}$ are set equal to zero – this imposes a soft XY constraint because the computation of the spin wave spectrum implicitly allows fluctuations out of the easy planes. This is relevant to the $\text{Er}_2\text{Ti}_2\text{O}_7$ pyrochlore antiferromagnet whose single-ion crystal field doublet, characterized by an anisotropic g -tensor with two eigenvalues such that $g_\perp > g_\parallel$, allows for a description in terms of an effective spin-1/2 model.²⁹ Working in reciprocal space with N spins and N_P primitive lattice sites, one rewrites the spin Hamiltonian in terms of boson operators, with^{21,22}

$$\tilde{S}_a^z(\mathbf{k}) = \sqrt{N_P} S \delta_{\mathbf{k},0} e^{-i\mathbf{k} \cdot \mathbf{r}_a} - \frac{1}{\sqrt{N_P}} a_a^\dagger(\mathbf{k}') a_a(\mathbf{k}' - \mathbf{k}) \quad (10)$$

$$\tilde{S}_a^x(\mathbf{k}) = \sqrt{\frac{S}{2}} (a_a^\dagger(\mathbf{k}) + a_a(-\mathbf{k})) \quad (11)$$

$$\tilde{S}_a^y(\mathbf{k}) = i\sqrt{\frac{S}{2}} (a_a^\dagger(\mathbf{k}) - a_a(-\mathbf{k})), \quad (12)$$

on each site with the new z axis now taken to be the quantization axis. The quantization axis is taken within the ground state manifold of the model with antiferromagnetic exchange as parametrized by local angles $\bar{\phi}_a$ for $a = 1, 2, 3, 4$ given in Eq. (2). There are four flavors of bosons corresponding to the distinct sublattices labelled with subscript a . One performs a Bogoliubov transformation taking boson operators $a_a^\dagger(\mathbf{k})$ and $a_a(\mathbf{k})$ into spin wave creation and annihilation operators

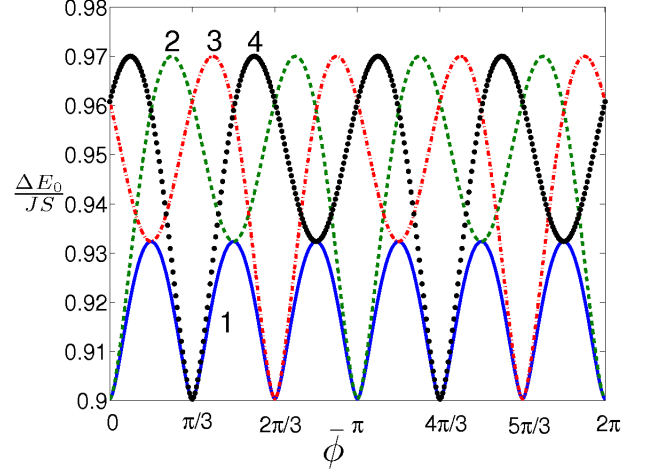


FIG. 2: (Color online) Zero point energy for the pyrochlore XY model from the linear spin wave spectrum computed from the classical ground states. The horizontal axis is the $\bar{\phi}$ parameter given in Eq. (2) and each curve carries a label identifying the branch of ground states to which it belongs. The quantum correction to the classical ground state energy is minimized for the ψ_2 states.

$c_A^\dagger(\mathbf{k})$ and $c_A(\mathbf{k})$ so that the Hamiltonian to harmonic order is brought to the form

$$H[\bar{\phi}] = -NJS(S+1) + JS \sum_{\mathbf{k},A} \epsilon_A(\mathbf{k}) + JS \sum_{\mathbf{k},A} \epsilon_A(\mathbf{k}) c_A^\dagger(\mathbf{k}) c_A(\mathbf{k}) \quad (13)$$

where $\epsilon_A(\mathbf{k})$ are the spin wave energies. Further details of Holstein-Primakoff linear spin waves on a pyrochlore lattice of spins can be found in Ref. [21]. As one would expect for an antiferromagnet, the dispersion for the model Eq. (1) about the zero modes is linear in $|\mathbf{k}|$. Just as in the classical case, the zero modes appear in pairs of planes in the first Brillouin zone for the ψ_2 states. The harmonic correction to the ground state energy is

$$N\Delta E_0[\bar{\phi}] \equiv \left(\frac{NJS}{4} \times \frac{1}{4} \right) \sum_A \int_{\text{BZ}} \frac{d^3\mathbf{k}}{(2\pi)^3} \epsilon_A(\mathbf{k}) \quad (14)$$

which we have evaluated numerically. The results are shown in Fig. 2. To harmonic order, one observes that, among the $\mathbf{q} = 0$ ground states, the zero point energy is minimized at the ψ_2 spin configurations ($\bar{\phi}_a = n\pi/3$ for all a), so a quantum order-by-disorder mechanism selects the same states as thermal fluctuations.

C. Monte Carlo results

To confirm the thermal order-by-disorder mechanism argued for in Section IV A, and to investigate further the concern, expressed in Ref. [15], that the ψ_2 long-range order

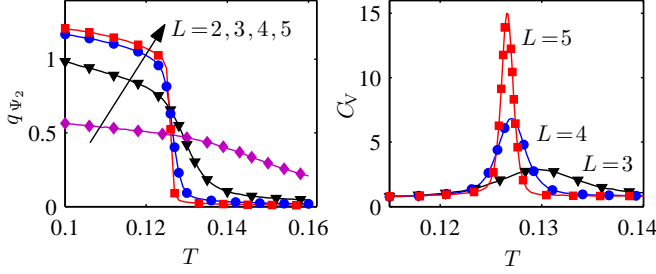


FIG. 3: (Color online) Order parameter q_{ψ_2} and heat capacity C_V as a function of temperature for $J = 1$ and $D = 0$. Left and right panels display results for q_{ψ_2} ($L = 2, 3, 4, 5$) and for C_V ($L = 3, 4, 5$), respectively.

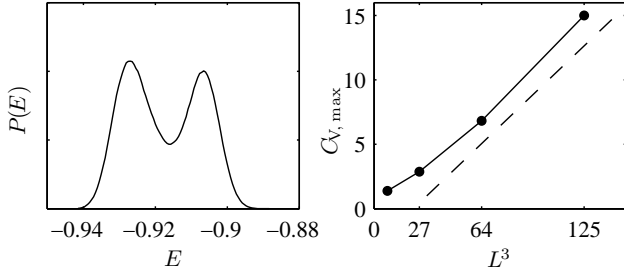


FIG. 4: (Color online) Two plots showing Monte Carlo data for $J = 1$ and $D = 0$ illustrating the first order nature of the transition. The left hand panel is a histogram of the measured energies for $L = 4$ at $T/J \simeq 0.127$, close to the transition temperature. The double-peaked structure is evidence for a coexistence region and hence an underlying first order transition. The right panel shows the peak height of the specific heat, $C_{V,\max}$, versus the cube of the system size, L^3 . The dash line shows a straight line for the hypothetical $C_{V,\max} \propto a + bL^3$ in the thermodynamic limit.

might not survive in the thermodynamic limit, we performed Monte Carlo simulations of the nearest neighbour exchange only model. Parallel tempering Monte Carlo simulation were carried out with $J = 1$ (and $D = 0$) for four different system sizes, $L = 2, 3, 4$ and 5 , of L^3 cubic unit cells of 16 spins. To equilibrate the system, 5×10^6 Monte Carlo sweeps were performed, followed by the same number of steps to collect data. All four system sizes were found to have equilibrated satisfactorily according to the criteria discussed in Sec. III. We note that we were unable to obtain well equilibrated results for $L = 6$ even using parallel tempering.

Figures 3, 4 and 5 show data from the Monte Carlo simulations for $D/J = 0$. The left hand panel of Fig. 3 shows the onset of the ψ_2 order parameter while the right panel shows the temperature dependence of the specific heat, C_V , near $T/J = 0.127$, the estimated transition temperature, for various system sizes. We have found that this estimated transition temperature $T_c/J \approx 0.127$ is consistent both with our sublattice magnetization results (not shown) and those of Ref. [15].

Both the rate of increase of the heat capacity peak and the jump in q_{ψ_2} with increasing L are consistent with a first order phase transition in the thermodynamic limit. The left hand

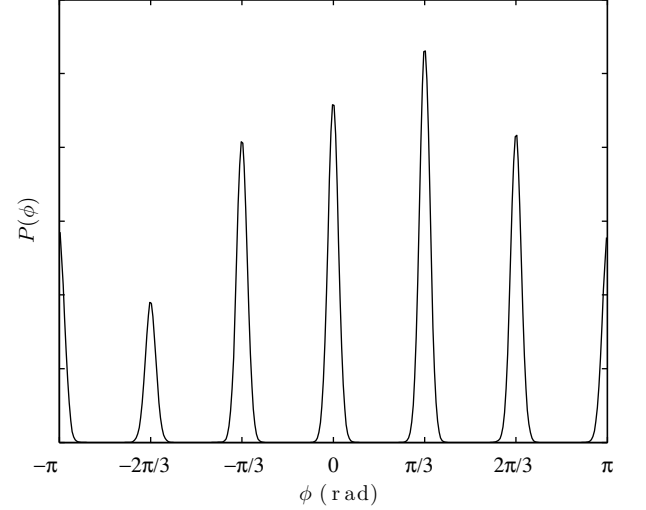


FIG. 5: Monte Carlo data for $J = 1$ and $D = 0$. Histogram of the local XY angles for all spins for $L = 4$ at a temperature $T/J = 0.1 \lesssim T_c$. The histogram shows peaks at angles $n\pi/3$ illustrating that the ψ_2 states are preferably sampled below $T_c/J \approx 0.127$.

panel of Fig. 4 is a histogram of the measured energies close to the transition temperature for $L = 4$. Its double-peaked structure is a clear indication of co-existence and hence of the first order nature of the transition. The right panel of Fig. 4 shows how the peak height of the specific heat, $C_{V,\max}$, depends on the the cube of the system size, L^3 . For a first order transition, one expects $C_{V,\max} \propto (a + bL^3)$ in the limit of large L .³⁰ The plot illustrates that for $L = 4$ ($L^3 = 64$) and $L = 5$ ($L^3 = 125$), $C_{V,\max}$ is approaching this expected behavior. This provides further evidence for a first order transition in this $D = 0$ $\langle 111 \rangle$ pyrochlore XY antiferromagnet. Finally, Fig. 5 shows a histogram of the local XY angle averaged over all spins on all sublattices at $T/J = 0.1$ for system size $L = 4$. The figure shows six sharp peaks concentrated at the ψ_2 angles $n\pi/3$. We find, in addition, that the spin angle on all sublattices are concentrated around one of these angles at any given Monte Carlo time. This result therefore demonstrates the selection of ψ_2 states from the continuous manifold of classical ground states and also that all six magnetic domains are sampled in the course of the simulation – a possibility facilitated by the use of a parallel tempering algorithm in our simulations compared to those of Refs. [13–15].

D. Further Cases of Order-by-Disorder in Pyrochlores

We have described in detail the nature of the ground states in the $\langle 111 \rangle$ XY pyrochlore antiferromagnet and how the classical degeneracy is resolved via an order-by-disorder mechanism. In contrast, the classical Heisenberg model on a pyrochlore lattice, which has a much less constrained set of ground states, exhibits no phase transition down to zero tem-

perature.¹² To put our results in the broader context of order-by-disorder in pyrochlore systems, we summarize in this short section two previously studied cases where the degeneracy of the Heisenberg antiferromagnet can be lowered by including additional interactions, leading to an entropic selection of a discrete state of long-range ordered states.

The first case is the pyrochlore Heisenberg model with both isotropic exchange and Dzyaloshinskii-Moriya (DM) interactions^{31,32}

$$H = J \sum_{\langle i,j \rangle} \mathbf{S}_i \cdot \mathbf{S}_j + \sum_{\langle i,j \rangle} \mathbf{D}_{ij} \cdot (\mathbf{S}_i \times \mathbf{S}_j).$$

Figure 2 in Ref. [31] gives the \mathbf{D}_{ij} which are completely determined by the lattice symmetry. We have taken a positive sign in front of the DM term to denote the so-called indirect DM couplings of Ref. [31]. In this case, the single tetrahedron ground states have four branches. One of these branches corresponds exactly to the equal $\bar{\phi}_a$ angle ground states of the $\langle 111 \rangle$ XY model [our Branch 1 of Eq. (2)]. The other three branches are coplanar spin configurations - the branches are distinguished by the three mutually perpendicular normals to these planes in the $\langle 100 \rangle$ crystallographic directions. The authors of Ref. [31] observed that Monte Carlo simulations at low temperatures lead to the selection of a discrete state of states - breaking down the continuous zero temperature classical degeneracy down to a Z_6 symmetry. In the notation convention of Ref. [18], these are the ψ_3 states. However, the nonzero temperature ordering turns out to be more complicated. As observed very recently in Ref. [32], upon lowering the temperature from the paramagnetic phase, there is a phase transition into a ψ_2 long-range ordered phase followed, at a lower temperature, by the ψ_3 ordering reported in Ref. [31]. This finding was confirmed within a harmonic Holstein-Primakoff computation of the free energy.³²

The second example of order-by-disorder we discuss is the Heisenberg pyrochlore antiferromagnet with both nearest-neighbor isotropic exchange and second neighbor interactions. When the second neighbor exchange is ferromagnetic, the finite temperature phase diagram explored by Monte Carlo³³ exhibits an intermediate phase that appears at intermediate temperatures between the collective paramagnet and the low temperature incommensurate multiple- \mathbf{q} ordered phase. This intermediate phase is partially ordered in the following sense. The magnetic structure is layered - each layer exhibiting collinear spins in one of three perpendicular axes \mathbf{n} which is common to all the layers. However, the orientation of the spins along the \mathbf{n} axis is apparently not correlated between the layers. The partially ordered phase is selected entropically as confirmed by a computation of the free energy.³³ The latter analytical calculation needs to, and does, include anharmonic terms to lowest order because, remarkably, the entropically selected intermediate phase is not a local minimum of the harmonic approximation to the free energy.

V. MATERIALS CONTEXT

A. $\text{Er}_2\text{Ti}_2\text{O}_7$

One motivation for our interest in the local easy plane pyrochlore antiferromagnet is the material $\text{Er}_2\text{Ti}_2\text{O}_7$. The Curie-Weiss temperature θ_{CW} of this material is negative³⁴ varying between -13 K and -22 K depending on the temperature range of measurement. $\text{Er}_2\text{Ti}_2\text{O}_7$ exhibits a transition at about $T_c = 1.2$ K.¹⁴ The ψ_2 magnetic structure of the ordered phase proposed in Ref. [14] has been confirmed by an analysis of polarized neutron scattering data.¹⁸

The spin wave spectrum has been measured recently³⁵ revealing the presence of an almost gapless mode at $\mathbf{q} = 0$ with a linear dispersion for small $|\mathbf{q}|$. This result is consistent with the T^3 magnetic specific heat trend with temperature T .^{14,39} The existence of a true Goldstone mode in this material is inconsistent with the selection of a discrete set of ordered states. The spin wave and specific heat experimental results must therefore be providing an upper bound on the size of the spin wave excitation gap in this material. Specifically, the inelastic neutron scattering spectrum in Ref. [35] can resolve the existence of a gap that is larger than about 1 K and the heat capacity measurements of Ref. [39] show that the heat capacity varies as T^3 down to the base temperature of 450 mK. One especially interesting feature of this material is that it apparently exhibits a field-driven quantum phase transition.³⁵ Application of a magnetic field in the $[110]$ direction below T_c causes a canting of the spins and leads to a zero mode in the vicinity of 1.5 T, which has been put forward as evidence for a finite field quantum phase transition in this material.^{35,36}

A greater understanding of the quantum critical point is likely to rely on a deeper understanding of the microscopic mechanism responsible for the zero field transition in this material. One difficulty with the local XY pyrochlore antiferromagnet as an effective model for $\text{Er}_2\text{Ti}_2\text{O}_7$ is that, unlike $\text{Er}_2\text{Ti}_2\text{O}_7$, the model exhibits a strong first order transition as we demonstrated in Section IV C.¹⁴ Another crucial difficulty is that the dipolar coupling of Er^{3+} ions is a significant perturbation to the estimated exchange.¹⁴ The dipolar interaction renders the ψ_2 structure energetically unstable and favors a distinct ground state, the ψ_4 (Palmer-Chalker) state, as pointed out originally in Ref. [14]. In the next subsection, we concentrate on the dipolar interaction as a perturbation to isotropic exchange interactions. Specifically, we consider the possibility that thermal order-by-disorder might persist in the presence of dipolar perturbations. After that, in Section IV C, we summarize the theoretical constraints that have been placed on the problem of understanding $\text{Er}_2\text{Ti}_2\text{O}_7$ in zero applied field.

B. Effect of competing dipolar interaction

In this section, we look at the effect of introducing pseudo-dipolar interactions on the order-by-disorder in the $\langle 111 \rangle$ XY pyrochlore antiferromagnet. We find that order-by-disorder into ψ_2 states survives for sufficiently small pseudo-dipolar

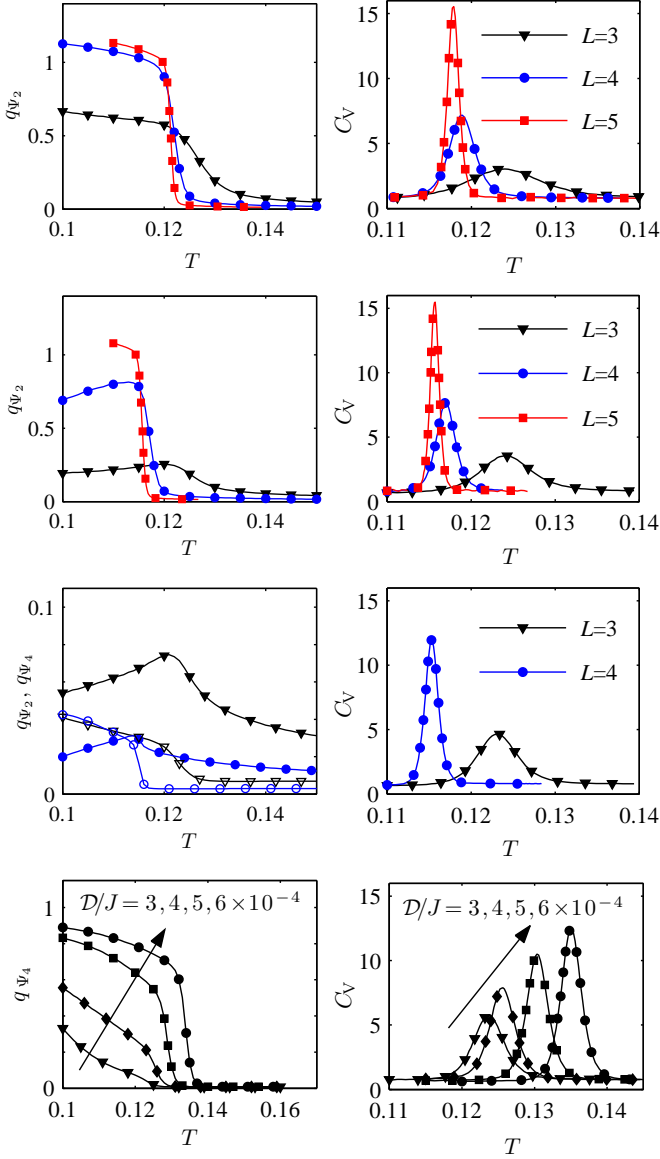


FIG. 6: (Color online) Figures showing the order parameters q_{ψ_2} and q_{ψ_4} and heat capacities for various values of \mathcal{D}/J . The top two rows, from top to bottom for $\mathcal{D}/J = 0.5 \times 10^{-4}$ and $\mathcal{D}/J = 10^{-4}$, show q_{ψ_2} and heat capacity data for $L = 3, 4, 5$. The third row down shows C_V and both q_{ψ_2} (solid symbols) and q_{ψ_4} (open symbols) for $\mathcal{D}/J = 2 \times 10^{-4}$ with $L = 3$ (down triangles) and $L = 4$ (circles) data. The bottom row of figures shows q_{ψ_4} and heat capacity data for $L = 3$ and $\mathcal{D}/J = 3, 4, 5, 6 \times 10^{-4}$, with \mathcal{D} increasing as indicated by the arrows.

couplings and estimate the maximum value of the dipolar coupling strength \mathcal{D} that permits ψ_2 ordering.

The dipolar interaction in the following is taken to act solely between nearest neighbors in order to reduce the difficulty in equilibrating the system and hence decrease the computer simulation time. We study this simplified model because (i) in combination with antiferromagnetic exchange, dipolar interactions between nearest neighbors select the same ψ_4 magnetic order as the long-range dipolar interactions²⁰ and be-

cause (ii) we have found, through preliminary simulations of Monte Carlo simulations of a model with long-range dipolar interaction (not reported), that the general conclusions of this subsection below do not depend sensitively on the range of these pseudo-dipolar interactions.

In order to examine the effect of dipolar perturbations on the thermal order-by-disorder mechanism, we carried out parallel tempering Monte Carlo simulations of the model with Hamiltonian (1) with nearest-neighbor dipolar interactions. With the introduction of these pseudo-dipolar interactions, the simulations were found not to equilibrate sufficiently for system sizes $L > 5$ for $\mathcal{D}/J \lesssim 10^{-4}$ and poor equilibration was found for $L > 4$ for $\mathcal{D}/J \gtrsim 10^{-4}$. The results presented in this section were obtained from simulations with 10^8 Monte Carlo sweeps of which the last 1/10th was used to compute the thermal averages after equilibration. Increasing the length of the simulations to 10^9 Monte Carlo sweeps was found neither to improve the results given below nor to achieve equilibration for larger system sizes than those presented below. The simulations were performed on SHARCNET using the Saw cluster with Intel Xeon 2.83GHz processors, with the $L = 5$ simulations requiring 10^8 Monte Carlo sweeps consuming ~ 17 CPU hours. Each simulation was run on 64 processors – one processor for each temperature.

Figure 6 shows the heat capacities and order parameters q_{ψ_2} and q_{ψ_4} for different values of \mathcal{D}/J (see Section III for a definition of q_{ψ_2} and q_{ψ_4}). The two top panels (left and right) show the results for $\mathcal{D}/J = 0.5 \times 10^{-4}$ for $L = 3, 4$ and 5 . There is a clear onset of the ψ_2 order parameter upon lowering the temperature and this feature becomes *sharper* when the system size increases. Similar behavior is shown in the second row down in Fig. 6 for a larger value, $\mathcal{D}/J = 10^{-4}$. The ψ_4 order parameter was also measured for these two values of \mathcal{D}/J and found to be close to zero, within the present finite size effects, and displaying no perceptible features around the onset temperature of q_{ψ_2} . This is, therefore, compelling evidence for the thermal order-by-disorder of an ordered ψ_2 state at nonzero temperature persisting in the presence of pseudo-dipolar interactions that break the ground state degeneracy in such a way that the thermally selected states are not the true ground states. The figures in the third row down (for $\mathcal{D}/J = 2 \times 10^{-4}$) reveal strong competition between ψ_2 and ψ_4 ordering as indicated by the fact that both order parameters are finite but small and suppressed upon increasing the system size. We were unable to obtain a clear signature of any long-range order in this region of pseudo-dipolar coupling in spite of the presence of a heat capacity peak that sharpens with increasing system size (right-hand panel, third row down). The bottom left-hand panel shows the ψ_4 order parameter for increasing \mathcal{D}/J showing the growing robustness of the transition to ψ_4 order as the pseudo-dipolar coupling is increased. For these values of \mathcal{D}/J , despite long runs of 10^9 Monte Carlo steps, the largest system size we were able to equilibrate was $L = 3$.

The dipolar coupling of nearest neighbor Er^{3+} moments in $\text{Er}_2\text{Ti}_2\text{O}_7$ is $\mathcal{D}/(2\sqrt{2})^3 = D_{\text{nn}} = \mu_0(g_J\mu_B)^2/4\pi R_{\text{nn}}^3 = 0.02$ K. Whether other (anisotropic) exchange interactions¹⁹ acting between the Er^{3+} ions are small compared to the

isotropic exchange is not known at this time (see Ref. [40] for a discussion of this problem for the $\text{Yb}_2\text{Ti}_2\text{O}_7$ XY pyrochlore).

Nevertheless, a fit to the local susceptibility of $\text{Er}_2\text{Ti}_2\text{O}_7$ in a [110] magnetic field of 1 T (see Ref. [41]) has yielded an order of magnitude estimate for the exchange coupling of about 10^{-1} K giving $(D_{\text{nn}}/J)_{\text{exp}} \sim 0.2$. On the other hand, Monte Carlo simulations gives an approximate boundary between the ψ_2 and ψ_4 long-range ordered phases of about $D/J \sim 2 \times 10^{-4}$ (see Fig. 6) or, in other words, a condition for the appearance of the ψ_2 phase of $D_{\text{nn}}/J \lesssim 0.005$. Therefore, one is faced with the following conundrum. For the experimental strength of the dipolar coupling and the estimated exchange coupling, the ordering transition in $\text{Er}_2\text{Ti}_2\text{O}_7$ should, according to our Monte Carlo simulations, take place into ψ_4 (Palmer-Chalker) states — but an ordering into ψ_2 states is observed experimentally. This highlights a problem with the thermal order-by-disorder scenario for $\text{Er}_2\text{Ti}_2\text{O}_7$.

C. Towards a model for $\text{Er}_2\text{Ti}_2\text{O}_7$

It is perhaps worth summarizing the physics problem associated with the zero field ordered state of $\text{Er}_2\text{Ti}_2\text{O}_7$. The long-range ordered magnetic structure that is experimentally observed in $\text{Er}_2\text{Ti}_2\text{O}_7$ arises via thermal order-by-disorder in the local $\langle 111 \rangle$ XY antiferromagnet, as discussed in Section IV. A large S expansion indicates, furthermore, that there is quantum order-by-disorder with the result that the ψ_2 states are ground states of this model. However, as we have shown in Section V B, the addition of a dipolar interaction (which is known to be present and relatively large in $\text{Er}_2\text{Ti}_2\text{O}_7$) is inconsistent with the selection of ψ_2 ordered states in the classical model. In order to resolve this paradox we might be led to consider the following possibilities: (i) quantum order-by-disorder overcomes the dipolar interaction as conjectured by Ref. [14], (ii) the nearest-neighbor bilinear exchange interaction is anisotropic^{19,40,41} and uniquely energetically selects a ψ_2 ordered state, (iii) there exist multipolar interactions between the Er^{3+} ions accounted for neither in the present work nor in previous ones,⁴² (iv) the crystal field is responsible for the effective anisotropy stabilizing the ψ_2 long-range ordered state¹⁹ and (v) that further neighbor interactions might be important in this problem.

It has been shown that allowing for anisotropic exchange interactions does not lessen the conceptual difficulties in understanding the ψ_2 ordering in $\text{Er}_2\text{Ti}_2\text{O}_7$.¹⁹ Specifically, as discussed in Ref. [19], no bilinear nearest-neighbor interactions in the idealized $\langle 111 \rangle$ XY model on a pyrochlore can bring about unique classical zero temperature ψ_2 ground states. The ψ_2 structure can be obtained, however, via local mean field theory by considering the full crystal field spectrum in addition to the anisotropic exchange. In this case, the effective single ion sixfold anisotropy arises from interaction-induced admixing of excited crystal field wavefunctions into the single ion ground state doublet.¹⁹ Unfortunately, even in this case, the strong long range dipolar interaction between Er^{3+} moments in $\text{Er}_2\text{Ti}_2\text{O}_7$ is expected to drive the system into a

different magnetically ordered (Palmer-Chalker) state, ψ_4 .²⁰ This is because the energetic selection produced by the dipolar interaction inherent to the Er^{3+} magnetic moments outweighs the six-fold single ion anisotropy effect above (that perturbs the XY-like single ion ground state doublet) by at least two orders of magnitude. The weakness of the ψ_2 selection proceeding via the involvement of the excited crystal field states is due to the large size of the crystal field gap ($\sim 10^2$ K¹⁴) compared to the perturbing interactions.¹⁹ In short, the combination of anisotropic exchange and crystal field effects do not appear to be able to win against the strong dipolar interactions and *energetically* stabilize the experimentally observed ψ_2 ^{14,18} state rather than the ψ_4 (Palmer-Chalker)²⁰ state. This would seem to rule out possibilities (ii) and (iv).

In addition, the existence of a ground state crystal field doublet separated from the first excited states by a gap much larger than the scale of the interactions implies that multipolar interactions between pairs of angular momenta in the microscopic model map to anisotropic bilinear exchange couplings¹⁹ in the low energy effective spin-1/2 theory,²⁹ thus seemingly ruling out multipolar interactions as the microscopic mechanism behind the zero field long-range order in $\text{Er}_2\text{Ti}_2\text{O}_7$.⁴⁴ Further neighbor interactions (which can also be anisotropic) have not yet been investigated.

We might consider instead a compromise between anisotropic exchange and thermal order-by-disorder — that important nearest-neighbor exchange anisotropy might more than cancel off the nearest-neighbor part of the interaction coming from the long-range dipolar interaction. The local XY antiferromagnet in the presence of pseudo-dipolar interactions with a coupling of the opposite sign [i.e. $\mathcal{D} < 0$ in Eq. (1)] to the physical long-range dipolar interaction preserves a continuous degeneracy that includes the discrete ψ_2 states.¹⁹ However, the degeneracy is reduced from the case with only exchange interactions. We might naively expect that the ψ_2 states will generically cease to be the configurations with the highest density of soft modes when such anisotropic interactions are introduced and hence that thermal order-by-disorder may not occur, at least not along the lines of the specific mechanism discussed in Section IV A. However, this naive reasoning may not be correct in general, as we now briefly mention.

An exception that was noted recently³² is the pyrochlore Heisenberg antiferromagnet with Dzyaloshinskii-Moriya interactions. As mentioned in Section IV D, Monte Carlo simulations and calculations of the free energy for that model reveal that ψ_2 states are entropically selected at intermediate temperatures between the high temperature paramagnet and a low temperature coplanar state. The effect of dipolar interactions was not investigated in Ref. [32]. However, one may speculate that in this, or some other model with anisotropic exchange, in the presence of dipolar interactions, ψ_2 states are selected as an intermediate temperature phase which remains as a metastable phase upon cooling. In other words, only one transition might be observed although two would be observed if the system were able to equilibrate.

The remaining possibility — that the ψ_2 states are the ground states of the quantum model despite strong dipolar interactions classically stabilizing a Palmer-Chalker ψ_4 state — is one

that has not yet been investigated. However, in the presence of the resulting strong and necessarily nonlinear (e.g. beyond $1/S$) quantum fluctuations, required to overcome the dipole-induced ψ_4 ground state, one might expect a substantial reduction of the ordered moment compared to the moment of the noninteracting doublet. This expectation contrasts with the experimental situation where the ordered moment is about $3\mu_B$ ¹⁴ compared to a noninteracting moment of $3.8\mu_B$ – a mere 20% reduction. Still, such an observation perhaps does not rule out quantum order-by-disorder which may therefore remains a possible solution to the problem of zero field ordering in $\text{Er}_2\text{Ti}_2\text{O}_7$ as originally conjectured in Ref. [14]. We hope that a future study will investigate the problem of the quantum ground state of the local $\langle 111 \rangle$ XY antiferromagnet in the presence of dipolar interactions perhaps by carrying out an anharmonic $1/S$ calculation of the ground state energy. Meanwhile, the microscopic mechanism that gives rise to a ψ_2 ordered phase at 1.2 K and with seemingly small quantum zero point fluctuations in $\text{Er}_2\text{Ti}_2\text{O}_7$ remains an open and interesting problem in the field of high frustrated magnetism.

In summary, no mechanism has yet been identified that can simultaneously explain how the (dipole-driven) energetic selection of the ψ_4 state is avoided in $\text{Er}_2\text{Ti}_2\text{O}_7$ while allowing for selection of the ψ_2 state below a critical temperature $T_c \sim 1.2$ K. This may indicate that quantum fluctuations do play a crucial role in the ψ_2 ordered state observed in $\text{Er}_2\text{Ti}_2\text{O}_7$ and that a renewed investigation of their effects is warranted.

VI. SUMMARY

We have presented in Sections II and IV, in some detail, the classical ground states, thermal and quantum behavior of the pyrochlore $\langle 111 \rangle$ XY antiferromagnet with exchange only. We have shown that the classical ground states on a single tetrahedron have four branches of ground states each with one continuous degenerate set of states involving the smooth rotation of all four spins simultaneously, confirming the previous result.¹⁵ From a calculation of the ground states on a single tetrahedron, we have inferred the ground states on the pyrochlore lattice which include line defects implying that the number of ground states scales as L^2 , where L is the edge length of the crystal.

Monte Carlo simulations of this model confirm that there is thermal selection of a discrete set of spin states, denoted ψ_2 states,¹⁸ with ordering wavevector $\mathbf{q} = 0$ from the manifold of classical ground states. We have shown, furthermore, that this selection occurs to harmonic order in small angular fluctuations about the classical ground states. In this model, the linear spin wave spectrum shows strong similarities with the spectrum of eigenvalues of the Hessian. Specifically, the spin wave zero modes and the Hessian zero modes appear within the same planes in reciprocal space for the ψ_2 states. It follows that the quantum zero point energy is minimized at the same ψ_2 spin configurations that are selected through a thermal order-by-disorder mechanism, hence confirming the conjecture of Refs. [14,15].

We have considered the effect of including (nearest-neighbor) pseudo-dipolar interactions together with the antiferromagnetic exchange in the classical model at finite temperature. The (energetically selected) ground states of this model are the ψ_4 states¹⁸ (also referred to as the Palmer-Chalker state²⁰), given in Section II, so the introduction of dipolar interactions produces a competition between energetic selection and thermal selection. We have found evidence for the persistence of an order-by-disorder transition to a ψ_2 state even when $\mathcal{D} \neq 0$. This finding implies that, in principle, a second transition should occur at lower temperatures into the ψ_4 (Palmer-Chalker) long-range ordered state since it is the classical ground state. However, using Monte Carlo simulations, we have found no evidence for such a transition, at the very least, because the difficulties of equilibration within the ordered ψ_2 phase prevent the exploration of the space of configurations computationally. A similar situation arises in a model that tunes between the Heisenberg pyrochlore antiferromagnet and the fcc Heisenberg antiferromagnet in which thermal order-by-disorder, studied using Monte Carlo simulations, prevails over the energetically driven ordering identified within mean field theory.⁴³ No transition was reported in Ref. [43] from the entropically selected ordered phase to the energetically favoured magnetic ordered phase. In contrast, the high and low temperature phase boundaries of an entropically stabilized intermediate (finite temperature) state have been identified in the J_1/J_2 pyrochlore Heisenberg antiferromagnet.³³

To conclude, we have shown that ψ_2 long-range order is present at low temperatures in the $\langle 111 \rangle$ XY pyrochlore antiferromagnet induced both by thermal and quantum fluctuations. How such ψ_2 states, either as a zero temperature ground state or as an ordered state at nonzero temperature, arise in the presence of (long-range) dipolar interactions remains an intriguing question that will require further theoretical investigation.

Acknowledgments

We thank Bruce Gaulin, Peter Holdsworth, Kate Ross, Jacob Ruff and Jordan Thompson for useful discussions. This research was funded by the NSERC of Canada and the Canada Research Chair program (M. G., Tier I). We acknowledge the use of the computing facilities of the Shared Hierarchical Academic Research Computing Network (SHARC-NET:www.sharcnet.ca).

Appendix A: Calculation of the Ground States of the XY Antiferromagnet

The zero moment conditions on a single tetrahedron are

$$\cos(\phi_1) + \cos(\phi_2) = \cos(\phi_3) + \cos(\phi_4) \quad (\text{A1})$$

$$\cos(\phi'_1) + \cos(\phi'_3) = \cos(\phi'_2) + \cos(\phi'_4) \quad (\text{A2})$$

$$\cos(\phi''_1) + \cos(\phi''_4) = \cos(\phi''_2) + \cos(\phi''_3), \quad (\text{A3})$$

where $\phi'_a \equiv \phi_a + \frac{2\pi}{3}$ and $\phi''_a \equiv \phi_a + \frac{4\pi}{3}$. The angles ϕ_a are angles in the local coordinate system on sublattice a ($a = 1, 2, 3, 4$). As discussed in Section II, and as previously reported in Ref. [16], the ground states of the $\langle 111 \rangle$ XY pyrochlore antiferromagnet are characterized by the following four set of solutions (“branches”):

$$\begin{aligned} \text{Branch 1 : } & \bar{\phi} \equiv \bar{\phi}_1 = \bar{\phi}_2 = \bar{\phi}_3 = \bar{\phi}_4 \\ \text{Branch 2 : } & \bar{\phi} \equiv \bar{\phi}_1 = \bar{\phi}_2 = -\bar{\phi}_3 = -\bar{\phi}_4 \\ \text{Branch 3 : } & \bar{\phi} \equiv \bar{\phi}_1 = \bar{\phi}_3, \quad \frac{2\pi}{3} - \bar{\phi} = \bar{\phi}_2 = \bar{\phi}_4 \\ \text{Branch 4 : } & \bar{\phi} \equiv \bar{\phi}_1 = \bar{\phi}_4, \quad \frac{4\pi}{3} - \bar{\phi} = \bar{\phi}_2 = \bar{\phi}_3. \end{aligned} \quad (\text{A4})$$

In this section, we present a derivation of this result that differs from the one in Ref. [16]. Defining $\sigma_{ab} \equiv (\phi_a + \phi_b)/2$ and $\delta_{ab} \equiv (\phi_a - \phi_b)/2$, we first proceed to rewrite the zero moment conditions as

$$\cos(\sigma_{12}) \cos(\delta_{12}) - \cos(\sigma_{34}) \cos(\delta_{34}) = 0 \quad (\text{A5})$$

$$-\sin(\sigma_{12}) \sin(\delta_{12}) + \sqrt{3} \cos(\sigma_{34}) \cos(\delta_{34}) = 0 \quad (\text{A6})$$

$$\sqrt{3} \cos(\sigma_{12}) \sin(\delta_{12}) - \sin(\sigma_{34}) \sin(\delta_{34}) = 0 \quad (\text{A7})$$

by using half-angle formulae and then combining the second and third zero moment conditions in Eq. (A3) to finally obtain Eqs. (A6) and (A7). Our strategy is to eliminate the sums of pairs, $\sigma_{\mu\nu}$, keeping only the differences of pairs, $\delta_{\mu\nu}$. Thus, from Eq. (A5), we get

$$\sin^2(\sigma_{12}) = 1 - \left(\frac{\cos(\sigma_{34}) \cos(\delta_{34})}{\cos(\delta_{12})} \right)^2$$

Substitute into Eq. (A6) to get

$$\begin{aligned} (1 - \sin^2(\delta_{12}) - \cos^2(\delta_{34}) \cos^2(\sigma_{34})) \sin^2(\delta_{12}) \\ = 3 \cos^2(\sigma_{34}) \sin^2(\delta_{34}) (1 - \sin^2(\delta_{12})) \end{aligned} \quad (\text{A8})$$

Then, squaring Eq. (A6) and Eq. (A7), and adding the result, we obtain

$$\sin^2(\delta_{12}) = \left(\frac{1}{3} \sin^2(\sigma_{34}) + 3 \cos^2(\sigma_{34}) \right) \sin^2(\delta_{34}) \quad (\text{A9})$$

which we can otherwise write as

$$\cos^2(\sigma_{34}) = \frac{3}{8} \left(\frac{\sin^2(\delta_{12})}{\sin^2(\delta_{34})} - \frac{1}{3} \right) \quad (\text{A10})$$

So now we can proceed with what we set out to do: substitute Eq. (A10) into Eq. (A8) leaving us, after re-arranging and cancelling off a $\cos^2(\delta_{12})$ term, with

$$\begin{aligned} \sin^2(\delta_{12}) \sin^2(\delta_{34}) = \\ \frac{1}{8} [3 \sin^2(\delta_{12}) - \sin^2(\delta_{34})] [3 \sin^2(\delta_{34}) + \sin^2(\delta_{12})] \end{aligned} \quad (\text{A11})$$

It follows from this last equation that

$$\frac{3}{8} (\sin^2(\delta_{34}) - \sin^2(\delta_{12})) = 0.$$

Hence, the most general form for the set of ϕ_a angles is

$$(\bar{\phi}_1, \bar{\phi}_2, \bar{\phi}_3, \bar{\phi}_4) = (\bar{\phi} + \theta, \bar{\phi}, \psi \pm \theta, \psi).$$

Substituting this into our original zero moment formula, Eq. (A5), which we write here again:

$$\cos(\bar{\phi}_1) + \cos(\bar{\phi}_2) = \cos(\bar{\phi}_3) + \cos(\bar{\phi}_4),$$

shows that one must have either

$$(\bar{\phi}_1, \bar{\phi}_2, \bar{\phi}_3, \bar{\phi}_4) = (\phi + \theta, \phi, \phi + \theta, \phi)$$

or

$$(\bar{\phi}_1, \bar{\phi}_2, \bar{\phi}_3, \bar{\phi}_4) = (\phi + \theta, \phi, \phi, \phi + \theta)$$

if θ is nonvanishing or

$$(\bar{\phi}_1, \bar{\phi}_2, \bar{\phi}_3, \bar{\phi}_4) = (\phi, \phi, \pm\phi, \pm\phi)$$

if $\theta = 0$. Thus, the angles must occur in pairs. One can now return to original zero moment conditions, Eq. (A3), and, with the knowledge that the angles must occur in pairs, obtain the four branches of ground states in Eq. (A4). For example, suppose that the pairs of angles occur in the configuration

$$(\psi, \phi, \phi, \psi)$$

then Eq. (A3) gives the branch

$$\left(\psi, \frac{4\pi}{3} - \psi, \frac{4\pi}{3} - \psi, \psi \right).$$

Appendix B: Brillouin Zone Integration

In the calculation of the free energy in Eq. (8), in particular the last term of that equation, we take the Brillouin zone sum over to an integral as applicable to the case of an infinite lattice. In general, we expect

$$\sum_{\mathbf{k}} \rightarrow \frac{N_P}{\Omega_{\text{BZ}}} \int_{\text{BZ}},$$

where the integral is taken over the Brillouin zone of volume Ω_{BZ} and N_P is the number of primitive cells. We thus have

$$\sum_{\mathbf{k}} \rightarrow \frac{Na^3}{4(4\pi)^3} \int_{\text{BZ}} d^3k.$$

The edge length of the cubic unit cell, a , has been set equal to one. The two factors of one quarter come about because (i) $4N_P = N$ where N is the number of spins and (ii) the Brillouin zone volume is $4(2\pi/a)^3$.

Appendix C: Equipartition argument

In this section, we revisit the Monte Carlo simulations presented in Ref. [15]. In particular, we consider Fig. 6 in that work showing the average energy in the ordered phase at low temperatures as a function of the system size. The authors of Ref. [15] found that

$$\frac{E}{Nk_B T} = \alpha - \beta \frac{1}{L}$$

We find that the existence of chains of zero modes in the $\langle 111 \rangle$ XY pyrochlore antiferromagnet is sufficient to constrain the coefficients α and β .

Let us consider a cubic cell with edge length L with each cubic unit cell of unit edge length. The number of spins is $N = 16L^3$. Consider a square face of a single cubic cell. There are two chains beginning on the face that alternate between sublattices a and b . The number of such chains passing through the sample is $N_{\text{chains}} = 2L^2$. There is one degree of freedom per spin so the average energy would be $(1/2)NkT$

were it not for the fact that the spectrum of modes about the ψ_2 states has planes of zero modes. We shall assume that the zero modes (in the harmonic spectrum) are actually resolved by a quartic contribution to the energy when looking at the higher order corrections to the Hamiltonian. The zero modes correspond to rotations along two classes of ab chains so the number of such modes is $2N_{\text{chains}}$. Thus, the average energy is

$$\frac{E}{k_B T} = \frac{1}{2} (N - 2N_{\text{chains}}) + \frac{1}{4} (2N_{\text{chains}}) = \frac{1}{2} N - \frac{1}{2} N_{\text{chains}}.$$

Then, because $N_{\text{chains}} = 2L^2 = 2(N/16)^{2/3}$, we obtain

$$\frac{E}{Nk_B T} = \frac{1}{2} - \frac{1}{16^{2/3}} N^{-1/3} = \frac{1}{2} - \frac{1}{16} \frac{1}{L}.$$

The coefficient in front of $1/L$ from Monte Carlo simulation¹⁵ is approximately 0.0636 which is in good agreement with the calculated $1/16 = 0.06250$ value above.

-
- ¹ G. H. Wannier Phys. Rev. **79**, 357 (1950); R. M. F. Houtappel, Physica **16**, 425 (1950).
 - ² S. T. Bramwell and M. J. P. Gingras, Science **294**, 1495 (2001).
 - ³ M. J. P. Gingras and B. C. den Hertog, Can. J. Phys. **79**, 1339 (2001).
 - ⁴ R. G. Melko and M. J. P. Gingras, J. Phys.:Condens. Matter **16**, R1277 (2004).
 - ⁵ S. V. Isakov, R. Moessner and S. L. Sondhi Phys. Rev. Lett. **95**, 217201 (2005).
 - ⁶ B. C. den Hertog and M. J. P. Gingras, Phys. Rev. Lett. **84**, 3430 (2000).
 - ⁷ H. Fukazawa, R. G. Melko, R. Higashinaka, Y. Maeno and M. J. P. Gingras Phys. Rev. B **65**, 054410 (2002); K. Matsuhira, Y. Hinatsu, K. Tenya and T. Sakakibara, J. Phys. Condens. Matter **12**, L649 (2000); J. Snyder, J. S. Slusky, R. J. Cava and P. Schiffer, Nature **413**, 48 (2001).
 - ⁸ J. Villain, Z. Phys. B **33**, 31 (1979).
 - ⁹ C. L. Henley, Phys. Rev. Lett. **62**, 2057 (1992).
 - ¹⁰ E. F. Shender, Zh. Eksp. Teor. Fiz. **56**, 178 (1982); T. Yildirim, A. B. Harris and E. F. Shender, Phys. Rev. B **53**, 6455 (1996).
 - ¹¹ Refs. [8–10] discuss a small assortment of models that exhibit order-by-disorder of some variety.
 - ¹² R. Moessner and J. T. Chalker, Phys. Rev. Lett. **80**, 2929 (1998); *ibid.*, Phys. Rev. B **58**, 12049 (1998).
 - ¹³ S. T. Bramwell, M. J. P. Gingras and J. N. Reimers, J. Appl. Phys. **75**, 5523 (1994).
 - ¹⁴ J. D. M. Champion, M. J. Harris, P. C. W. Holdsworth, A. S. Wills, G. Balakrishnan, S. T. Bramwell, E. Čížmár, T. Fennell, J. S. Gardner, J. Lago, D. F. McMorrow, M. Orendáč, A. Orendáčová, D. McK. Paul, R. I. Smith, M. T. F. Telling and A. Wildes, Phys. Rev. B, **68**, 020401(R) (2003).
 - ¹⁵ J. D. M. Champion and P. C. W. Holdsworth, J. Phys. Condens. Matter, **16**, S665 (2004).
 - ¹⁶ J. D. M. Champion, Ph.D. Thesis. University of London (2001).
 - ¹⁷ J. S. Gardner, M. J. P. Gingras, J. E. Greedan, Rev. Mod. Phys. **82**, 53 (2010).
 - ¹⁸ A. Poole, A. S. Wills and E. Lelièvre-Berna, J. Phys. Condens. Matter, **19**, 452201 (2007).
 - ¹⁹ P. A. McClarty, S. H. Curnoe and M. J. P. Gingras, J. Phys.:Conf. Series **145**, 012032 (2009).
 - ²⁰ S. E. Palmer and J. T. Chalker, Phys. Rev. B **62**, 488 (2000).
 - ²¹ A. G. Del Maestro and M. J. P. Gingras, J. Phys.:Condens. Matter, **16**, 3339 (2004).
 - ²² A. G. Del Maestro and Michel J. P. Gingras, Phys. Rev. B **76**, 064418 (2007).
 - ²³ A. S. Wills, M. E. Zhitomirsky, B. Canals, J.P. Sanchez, P. Bonville, P. Dalmás de Reotier and A. Yaouanc, J. Phys.:Condens. Matter **18**, L37 (2006); J. R. Stewart, J. S. Gardner, Y. Qiu and G. Ehlers, Phys. Rev. B **78**, 132410 (2008).
 - ²⁴ J. R. Stewart, G. Ehlers, A. S. Wills, S. T. Bramwell and J. S. Gardner, J. Phys.: Condens. Matter **16**, 321 (2004); J. S. Gardner, J.R. Stewart and G. Ehlers, Neutron and X-ray scattering Advanced Materials Research, AIP Conference Proceedings **1202**, 3 (2009).
 - ²⁵ E. Marinari and G. Parisi, Europhys. Lett. **19**, 451 (1992); K. Hukushima and K. Nemoto, J. Phys. Soc. Jpn. **65**, 1604 (1996).
 - ²⁶ M. Enjalran and M. J. P. Gingras, Phys. Rev. B **70**, 174426 (2004).
 - ²⁷ O. Cépas, A. P. Young and B. S. Shastry, Phys. Rev. B **72**, 184408 (2005).
 - ²⁸ The free energy is a smooth function of the parameter that tunes between classical ground states despite the presence of zeros in the eigenvalues of the Hessian. This is because the zeros occur on planes in the Brillouin zone. Consider a plane of zeros in the yz plane with linear dispersion (for an antiferromagnet) giving a k_x dispersion for small k_x away from the plane of zeros. The free energy is, roughly, the integral over the Brillouin zone of $\log k_x$ or
$$\int_0^c dk_x \log |k_x|$$
where the upper (positive) limit is arbitrary. This integral is finite.
 - ²⁹ See the supplemental material in J. D. Thompson *et al.*, Phys. Rev. Lett. **106**, 187202 (2011) for a related discussion for the XY pyrochlore ferromagnet $\text{Yb}_2\text{Ti}_2\text{O}_7$.

- ³⁰ K. Binder and D. W. Heermann, *Monte Carlo Simulation in Statistical Physics*, Third Edition, Springer, Germany, (1997).
- ³¹ M. Elhajal, B. Canals, R. Sunyer, and C. Lacroix, Phys. Rev. B **71**, 094420 (2005).
- ³² G.-W. Chern, arXiv:1008.3038.
- ³³ G.-W. Chern, R. Moessner and O. Tchernyshyov, Phys. Rev. B **78**, 144418 (2008).
- ³⁴ S. T. Bramwell, M. N. Field, M. J. Harris and I. P. Parkin, J. Phys. Condens. Matter, **12**, 483 (2000); P. Dasgupta, Y. Janab and D. Ghosh, Solid State Comm., **139**, 424 (2006).
- ³⁵ J. P. C. Ruff, J. P. Clancy, A. Bourque, M. A. White, M. Ramazanoglu, J. S. Gardner, Y. Qiu, J. R. D. Copley, M. B. Johnson, H. A. Dabkowska and B. D. Gaulin, Phys. Rev. Lett. **101**, 147205 (2008).
- ³⁶ We note, however, that similarly to the behavior of $\text{Gd}_2\text{Ti}_2\text{O}_7$ in a field³⁷, perhaps also in $\text{Gd}_2\text{Sn}_2\text{O}_7$ ³⁸, it would seem plausible that $\text{Er}_2\text{Ti}_2\text{O}_7$ many exhibit several field driven transitions from its zero field state to its highly polarized state at $\gtrsim 5 - 10$ T (see Ref. [35]). For example, a calculation that considers the effect of a [110] field in a microscopic model of $\text{Er}_2\text{Ti}_2\text{O}_7$ does find evidence for multiple field-driven transitions (see Ref. [19]).
- ³⁷ A. P. Ramirez, B. S. Shastry, A. Hayashi, J. J. Krajewski, D. A. Huse and R. J. Cava, Phys. Rev. Lett. **89**, 067202 (2002).
- ³⁸ R. S. Freitas and J. S. Gardner, J. Phys.: Condens. Matter **23**, 164215 (2011).
- ³⁹ S. S. Sosin, L. A. Prozorova, M. R. Lees, G. Balakrishnan and O. A. Petrenko, Phys. Rev. B **82**, 094428 (2010).
- ⁴⁰ J. D. Thompson, P. A. McClarty, H. M. Rønnow, L. P. Regnault, A. Sørge and M. J. P. Gingras, Phys. Rev. Lett. **106**, 187202 (2011).
- ⁴¹ H. Cao, A. Gukasov, I. Mirebeau, P. Bonville, C. Decorse and G. Dhalenne, Phys. Rev. Lett. **103**, 056402 (2009).
- ⁴² P. Santini, S. Carretta, G. Amoretti, R. Caciuffo, N. Magnani and G.H. Lander, Rev. Mod. Phys. **81**, 807 (2009).
- ⁴³ C. Pinettes, B. Canals and C. Lacroix, Phys. Rev. B **66**, 024422 (2002).
- ⁴⁴ In more detail, suppose that the microscopic interactions between magnetic ions are two-body interactions that respect the lattice symmetries. Suppose, furthermore, that the crystal field spectrum has a ground state doublet and a gap to excited single ion states, Δ , that is much larger than the energy scale associated with the interactions. Finally, we suppose that we are interested in temperatures $T \ll \Delta$. Then the excited crystal field can be neglected and the effective theory at low energies is the projection of the microscopic Hamiltonian onto the product of crystal field doublets on each magnetic ion. Since the space of states at each magnetic site is two dimensional, all site operators are linear combinations of Pauli spin operators regardless of the nature of the bare microscopic interactions. Therefore multipolar interactions project onto bilinear exchange couplings.